

Expansion behavior of low-strength steel slag mortar during high-temperature catalysis

Wen-Ten Kuo^{*} and Chun-Ya Shu^a

Department of Civil Engineering, National Kaohsiung University of Applied Sciences, No. 415, Chien-Kung Rd., Sanmin District, Kaohsiung 80778, Taiwan, R.O.C.

(Received June 16, 2015, Revised July 13, 2015, Accepted July 18, 2015)

Abstract. This study established the standard recommended values and expansion fracture threshold values for the content of steel slag in controlled low-strength materials (CLSM) to ensure the appropriate use of steel slag aggregates and the prevention of abnormal expansion. The steel slags used in this study included basic oxygen furnace (BOF) slag and desulfurization slag (DS), which replaced 5-50% of natural river sand by weight in cement mixtures. The steel slag mortars were tested by high-temperature (100°C) curing for 96 h and autoclave expansion. The results showed that the effects of the steel slag content varied based on the free lime (f-CaO) content. No more than 30% of the natural river sand should be replaced with steel slag to avoid fracture failure. The expansion fracture threshold value was 0.10%, above which there was a risk of potential failure. Based on the scanning electron microscopy (SEM) analysis, the high-temperature catalysis resulted in the immediate extrusion of peripheral hydration products from the calcium hydroxide crystals, leading to a local stress concentration and, eventually, deformation and cracking.

Keywords: high-temperature catalysis; basic oxygen furnace slag; desulfurization slag; controlled low-strength materials; volume stability behavior

1. Introduction

In recent years, natural sandstone has been excessively exploited in Taiwan, and the demand largely exceeds the supply. The natural resources are being exhausted due to numerous engineering constructions, and the solution is to find replacement resources. The steel industry is associated with large-scale industrial sites in various regions. The iron and steel manufacturing process consumes a large amount of resources and energy and produces various byproducts and wastes. These byproducts can be used as mixing materials (Qasrawi 2009, Lun *et al.* 2008). Despite the uncertainty in the available references and estimations, the world steel industry produced 1.5 billion tonnes of steel in 2012 (World steel Association 2013). The amount of slag waste generated is calculated to be between 10% and 20% of the raw material used (depending on the quality of the

^{*} Corresponding author, Professor, E-mail: wtkuo@cc.kuas.edu.tw

^a Ph.D. candidate, E-mail: chunya@hcv.s.kh.edu.tw

metal, oxide content, oxygen supply volume and furnace efficiency) (Rodriguez *et al.* 2013). In Taiwan, the annual output of basic oxygen furnace (BOF) slag and desulfurization slag (DS), which are major sources of industrial waste, is approximately 1.6 million tons, accounting for 25% of the mainsolid waste. Appropriate use of these wastes can reduce the amount of waste in landfills and the excessive consumption of natural resources. However, too high free lime may affect both mechanical properties and durability of concrete (Cengiz *et al.* 2004, Vagelis 2000). The non-water granulated furnace slag eventually expands because of its lime and magnesia contents. To avoid the expansion, these contents must be reduced to below 2-3%; otherwise, the slag will not be useful (Svanera 2012). After these solid wastes are stabilized using certain procedures (Rafat 2009), they can be used as controlled low-strength materials (CLSM) aggregates, thus increasing the waste material reutilization efficiency, reducing environmental pollution and damage and the waste of natural resources and creating profits (Sivakumar *et al.* 2012, Naganathan *et al.* 2010). In many studies, the furnace slag has been used as concrete (Lizarazo-Marriaga *et al.* 2011, Chen 2011, Wang *et al.* 2014), roadbed (Wu *et al.* 2007, Wang and Emery 2004) or asphalt aggregates (Shen *et al.* 2009). However, the material properties are difficult to control due to the material processing, quality control and material instability. Inappropriate use of the aggregates can result in their abnormal expansion, leading to pavement upheaval and damage (Ivanka 2011). The present specifications emphasize the strength and workability of the material. But durability is affected by the abnormal expansion behavior and its instability over time, is neglected. Multiple cases of cracking and expansion after aggregate backfill have been observed in Taiwan and abroad (Hwang 2010). Wang *et al.* (Wang 2010, Wang *et al.* 2010, Mahmoud 2012) indicated that the hydrated oxides CaO and MgO in the steel slag might impact the volume stability. The steel slag must be stabilized, controlled, tested and treated appropriately to make it useful in engineering applications, f-CaO and f-MgO cause the expansion failure of backfill pavement because curing at normal temperatures does not allow for the hydration of the oxides, and abnormal expansion occurs only after a long time (Li and Li 2005). The main factor which is governing the expansion is the free CaO and MgO contents in cement. The expansion is due to the formation of Ca(OH)_2 and Mg(OH)_2 upon the delayed hydration of free CaO and MgO respectively (Tareq and Attar 2013). Chatterji (Chatterji 1995) stated that the mechanism of expansion for both oxides is the same, and its capacity for free CaO is more due to that Ca(OH)_2 is more soluble than Mg(OH)_2 . These hydration mechanisms mostly occur after general concrete hardening, resulting in the expansion failure of the concrete. This study used tropical curing to evaluate the relationship between the content and expansion behavior of BOF and DS in a CLSM cement mortar. Hence, the suitability of the material for use in different engineering applications can be known before it is used extensively, thus avoiding problems with the engineering quality and even threats to user safety.

2. Materials and methods

2.1 Materials and mix proportions

The BOF and DS used in this study were produced by China Steel Corp. (Taiwan) and broken and screened by downstream firms. The particle size of the fine aggregate was 0-5 mm, according to hazardous industrial waste standard, the toxicity characteristic leaching procedure (TCLP) dissolution test was performed to ensure that the concentrations of dissolved heavy metals were

Table 1 Chemical Analysis and Physical Characteristics of BOF and DS Slag

Oxides	Chemical analysis (%)	
	BOF	DS
SiO ₂	16.68	17.57
Al ₂ O ₃	0.38	5.90
Fe ₂ O ₃	25.38	12.61
CaO	50.93	56.82
MgO	—	—
K ₂ O	0.09	0.01
Na ₂ O	—	—
SO ₃	—	3.55
Cr ₂ O ₃	—	0.14
TiO ₂	0.38	—
Free CaO	3.24	15.95
	<i>Physical characteristics</i>	
Specific gravity	3.04	2.17
Absorption (%)	5.7	21.5

Table 2 Mixture Proportions of Steel Slag Mortar (Unit: kg/m³)

Item	Cement	Water	Sand	BOF	DS
Ref.	200	300	1674	-	-
BOF 05	200	300	1590	83	-
BOF 10	200	300	1506	167	-
BOF 20	200	300	1339	334	-
BOF 30	200	300	1171	502	-
BOF 40	200	300	1004	669	-
BOF 50	200	300	837	837	-
DS 05	200	300	1590	-	83
DS 10	200	300	1506	-	167
DS 20	200	300	1339	-	334
DS 30	200	300	1171	-	502
DS 40	200	300	1004	-	669
DS 50	200	300	837	-	837



Fig. 1 Rupture area quantified example

within the prescribed limits. The material was identified as safe leaching concentration. Wang *et al.* (Wang 2010, Mahmoud 2012) Steel slag contains free (unhydrated) lime (CaO) that can result in volumetric instability (expansion). Table 1 shows the chemical and physical properties of the BOF and DS. X-ray fluorescence (XRF) was used to determine the slag components, which included SiO₂, Fe₂O₃ and CaO. The free lime content was high. The hydration of free lime to form Ca(OH)₂

is one of the important causes of expansion (Chaurand *et al.* 2007, Motz and Geiseler 2001, Shi and Qian 2000), and lengthy periods of time are required to achieve the potential expansion of slag because of the hydration of certain aluminates and calcium oxide in addition to the slow hydro carbonation reactions of magnesium oxide (Montenegro *et al.* 2013). Type I cement (Taiwan Cement Corp.), whose properties conformed to ASTM C114-05, was used in this study. The natural river sand conformed to ASTM C33. The cement:natural river sand:water mix ratio was 1:8.37:1.5, and controlled low-strength material (CLSM) cement mortar was produced by replacing 0%, 5%, 10%, 20%, 30%, 40% and 50% of the natural river sand by weight with the steel slag. The mortar mix ratios are summarized in Table 2.

2.2 Methods

Due the free lime may also be encapsulated inside particle during the formation process (Krittiya *et al.* 2013). Therefore the use of high-temperature catalysis accelerated expansion behavior. To examine the expansion of the BOF and DS during high-temperature catalysis, cement mortars $2.54 \times 2.54 \times 28.5 \text{ cm}^3$ in size were made with different ratios of the various components. Two high-temperature test methods, autoclave expansion and heating catalysis, were used for the catalysis. The area of expansion failure was quantified using the square method to compare the amount of damage for the different samples. Finally, the hydration inside the sample was observed by SEM microscopic analysis. The autoclave expansion conformed to ASTM C151. The heating catalysis was performed by placing the specimen in a constant temperature and humidity curing cabinet for tropical curing at a temperature of 100°C and relative humidity of 100%. The specimen was removed every 24 h to measure its length and record the SEM image. The area of the specimen that was damaged (damage area) was quantified using a transparent grid, and then, the specimen was placed in the constant temperature and humidity curing cabinet again. The tropical curing was stopped after 4 days of repeated action. The damage area was quantified using a computer and transparent grid to measure the damage in four planes of the specimen. The small grid area was $1 \text{ mm} \times 1 \text{ mm}$, and each side of the mortar bar had 7,125 small grids; thus, the four sides had a total of 28,500 grids. As shown in Fig. 1, the sample failure points, planes and cracks were put on the grids for quantification, and the damage area percentage was calculated using Eq. (1).

$$\text{rupture area}(\%) = \frac{\sum \text{rupture cells}}{28500} \times 100 \quad (1)$$

Study using two high-temperature test methods to find out the effect of temperature on the expansion. The area of the specimen that was damaged (damage area) was quantified using a transparent grid to examine extent of the damage. Steel slag replace, high-temperature catalysis and curing time relevance, all together presented in the article.

3. Results and discussion

3.1 Autoclave expansion

Fig. 2 shows the volume expansion capacity of low-strength mortar with different amounts of slag after the autoclave expansion. When the BOF replaced less than 10% of the natural river sand,

the expansion capacity was 0.090%, which was higher than that of the control group (0.048%). When 20% of the natural river sand was replaced by the BOF, the expansion capacity was as high as 0.120%. Cracks were observed in the mortar due to the expansion. When more than 30% of the natural river sand was replaced with BOF, fracturing and deformation were observed, and the measurement failed to continue. When DS replaced 10% of the natural river sand, the expansion capacity was 0.110%, which was much higher than the expansion capacity when the BOF was used. When more than 20% of the natural river sand was replaced with DS, fracturing occurred directly, and the expansion capacity could not be measured. Show the high free lime content tends to cause higher autoclave expansion (Krittiya *et al.* 2013). Fig. 3 shows the photo image of the sample with 20% BOF. The sample was cracked and damaged severely.

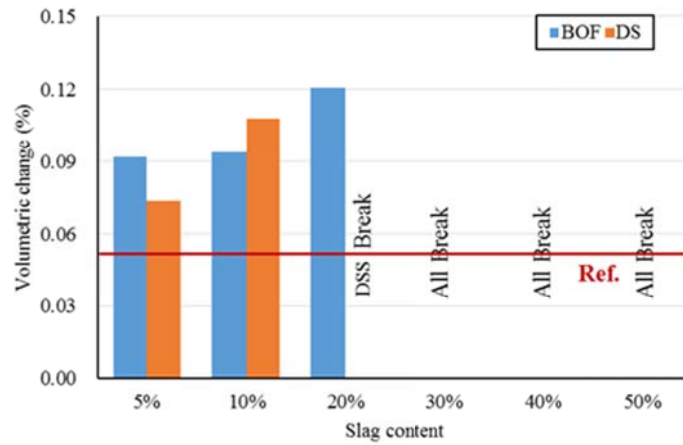


Fig. 2 The volume expansion capacity of low-strength mortar with different amounts of slag after the autoclave expansion



Fig. 3 The photo image of the sample with 20% BOF (after the autoclave expansion)



Fig. 4 The photo image of the sample with 30% DS (after the autoclave expansion)

White powdered crystals were observed after peeling off the cracks. Fig. 4 shows the photo image of the sample with 30% DS. Severe point-like bursts were observed on the surface, and the sample was severely fractured. White powdered crystals were also detected on the failure plane of this sample. The XRD analysis showed that the principal components of the white crystals were $\text{Ca}(\text{OH})_2$ and $\text{Mg}(\text{OH})_2$. If the free calcium or magnesium oxides (CaO or MgO , respectively) came into contact with water, their hydrated products formed tufa. Tufa is a spongy, porous mineral precipitate that is fragile and crumbles easily. If a slag contains a significant fraction of either free lime (CaO) or magnesia (MgO), it can expand if moistened, which could cause any paving, foundations or walls located above the slag to buckle or heave [Beaver Valley Slag]. Based on these results, when the expansion value was higher than 0.10%, the potential for damage was high, and point-like bursts or direct fractures could form. The use of excessive steel slag would cause destructive expansion.

3.2 Heating catalysis

Fig. 5 shows the volume expansion capacity of the mortar with different amounts of DS after high-temperature catalysis. After the 10% DS sample underwent 48 h of catalysis, the expansion capacity was 0.10%, and a burst trace began to occur on the sample surface. The burst and expansion capacity increased with the catalysis time. The expansion capacity of the 10% DS sample was 0.13% after 96 h, and the 20% DS sample fractured after 48 h of catalysis. Fig. 6 shows the damage area ratios of the low-strength mortar with different amounts of DS after high-temperature catalysis. When DS replaced 10% of the natural river sand, the surface fracture increased continuously with the catalysis time. The damage area ratio was as high as 1.10% after 96 h. The samples with a DS content higher than 30% fractured after 24 h of catalysis, and the failure surface area could not be quantified. Fig. 7 shows the failure images of the mortars with different amounts of DS over time during the high-temperature catalysis. Figs. 7(a) and 7(b) show that the failure mostly occurred in corners for the 10% DS sample. Fig. 7(c) shows that when 20% of the natural river sand was replaced with DS, the expansion capacity increased after 24 h of catalysis, and a point-like burst was observed. Fig. 7(d) shows that fracturing occurred at 48 h, and no further measurements were performed. Fig. 8 shows the results for the mortars with different

amounts of BOF. The expansion capacity was 0.05% after 96 h of catalysis for the 5% BOF sample, and no burst or failure was observed at the specimen surface. When BOF replaced more than 10% of the natural river sand, the expansion capacity increased with the catalysis time. For the 30% BOF sample, fracturing occurred after 72 h of catalysis, and no further measurements were performed. The results showed that the replacement aggregate expanded when the expansion capacity was greater than 0.05%, and the risk of potential failure was high for expansion capacities greater than 0.10%. Fig. 9 shows the damage area ratios of the low-strength mortars with different amounts of BOF after high-temperature catalysis. The damage area ratio was lower than 0.60% after 96 h of catalysis for the 10% BOF sample. When 20% of the natural river sand was replaced by BOF, the failure surface area was almost 0.70% after 96 h. When BOF replaced 30% of the natural river sand, the surface fractured in several places after 48 h of catalysis, and the damage area ratio was higher than 0.6%. Therefore, when the damage area ratio was 0.70%, the BOF mortar might have failed. Fig. 10 shows the failure images of the mortars with different amounts of BOF over time during high-temperature catalysis. Fig. 10(a) shows the image of the 20% BOF sample after 48 h of catalysis. Point-like prominent cracks were observed near the corners. Fig. 10(b) shows the image of the 30% BOF sample after 48 h of catalysis. White powdered crystals were observed in the corners of the screw side, and severe failure was detected. Fig. 10(c) shows the image of the 30% BOF sample after 72 h of catalysis. Severe fracturing occurred, and white powdered crystals were found in the cracks. Fig. 10(d) shows the image of the 10% BOF sample after 96 h of catalysis. Extensive spalling occurred, and white powdered crystals were observed in the failure. In contrast to the samples with higher BOF contents, this phenomenon occurred locally.

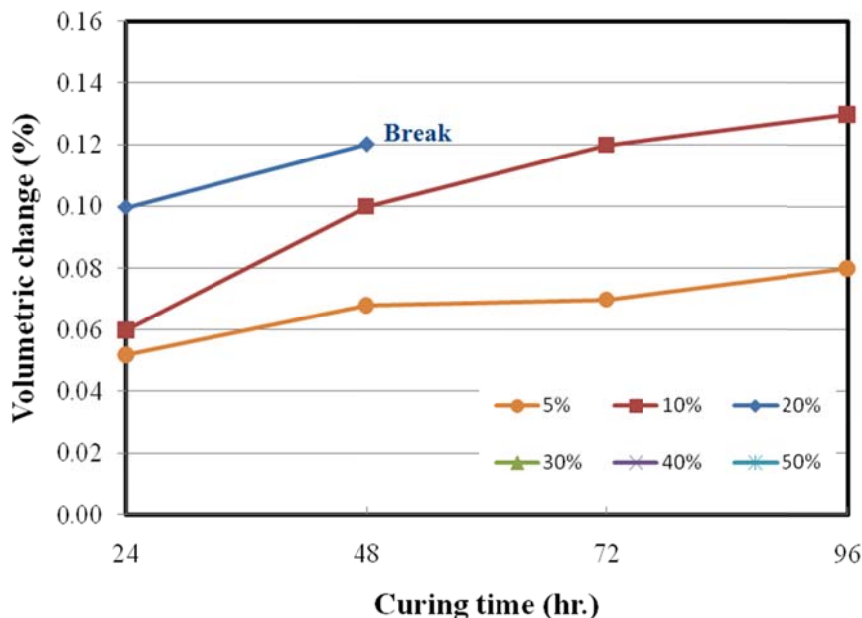


Fig. 5 The volume expansion capacity of the mortar with different amounts of DS after high-temperature catalysis (30%~50% of the samples, after 24 hours catalytic samples have been break, cannot be measured)

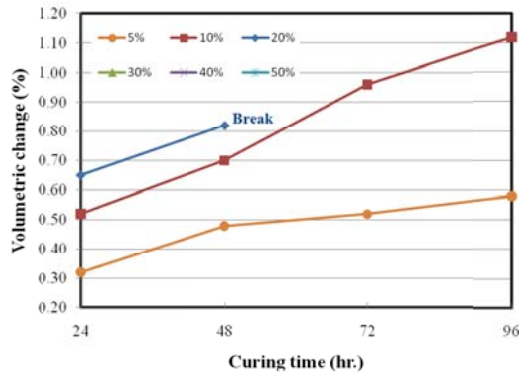


Fig. 6 The damage area ratios of the low-strength mortar with different amounts of DS after high-temperature catalysis (30% ~50% of the samples, after 24 hours catalytic samples have been break, cannot be measured)

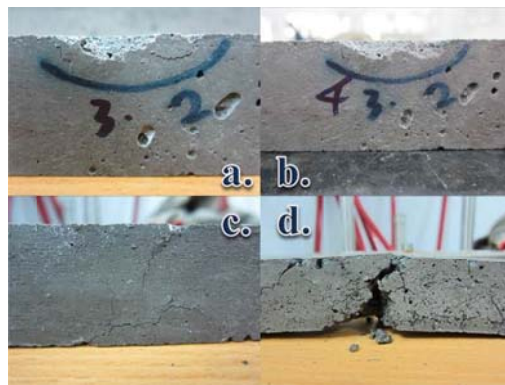


Fig. 7 The failure images of the mortars with different amounts of DS over time during the high-temperature catalysis (a) 10%, 72 hr, (b)10%, 96 hr, (c) 20%, 24 hr, (d)20%, 48 hr

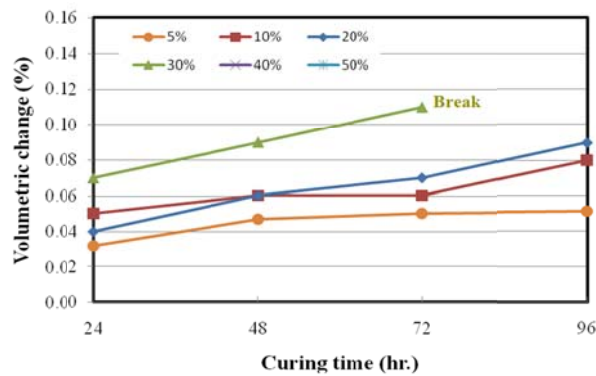


Fig. 8 The results for the mortars with different amounts of BOF (40%~50% of the samples, after 24 hours catalytic is break)

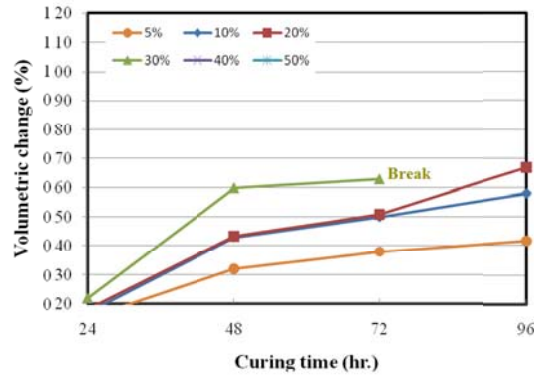


Fig. 9 The damage area ratios of the low-strength mortars with different amounts of BOF slag after high-temperature catalysis (40%~50% of the samples, after 24 hours catalytic is break)

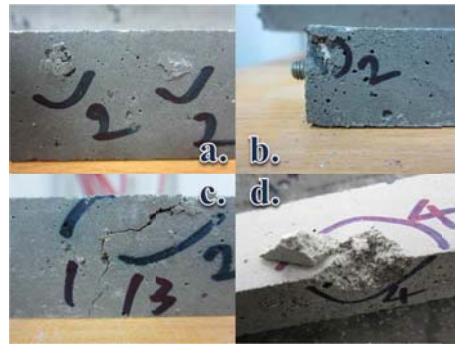


Fig. 10 The failure images of the mortars with different amounts of BOF slag over time during high-temperature catalysis (a) 20%, 48 hr, (b) 30%, 48 hr, (c) 30%, 72 hr, (d) 10%, 96 hr

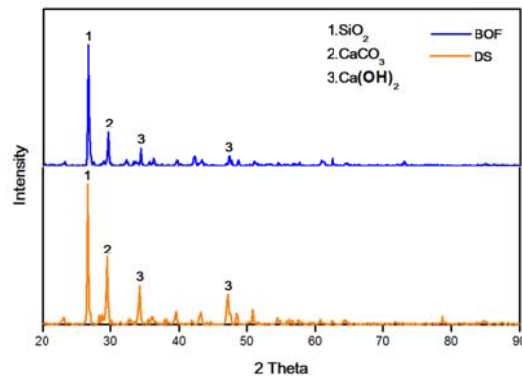


Fig. 11 XRD of the BOF slag and DS slag

3.3 X-ray diffraction (XRD)

The BOF and DS were analyzed by X-ray diffraction (XRD), and the results are shown in Fig.

11. The principal component of the two steel slags was found to be a Ca-based constituent. The relatively large peaks were due to $\text{Ca}(\text{OH})_2$, CaCO_3 and SiO_2 . The main constituent of the natural river sand was SiO_2 , and a small amount of KAlSi_3O_8 was also detected (Wang 2008). The Ca content, however, was insignificant. In contrast, the steel slag contained more $\text{Ca}(\text{OH})_2$ but less SiO_2 . The natural river sand exhibited high chemical stability because of its high SiO_2 content (Wang 2008). However, the steel slag had lower chemical stability because of its higher $\text{Ca}(\text{OH})_2$ content, which led to the expansion failure. In addition, the peak strength of DS was higher than that of BOF, meaning that the DS steel slag aggregate was more unstable than the BOF aggregate. Based on the real expansion values and damage area ratios, the DS samples underwent greater expansion and exhibited more failure than the BOF samples.

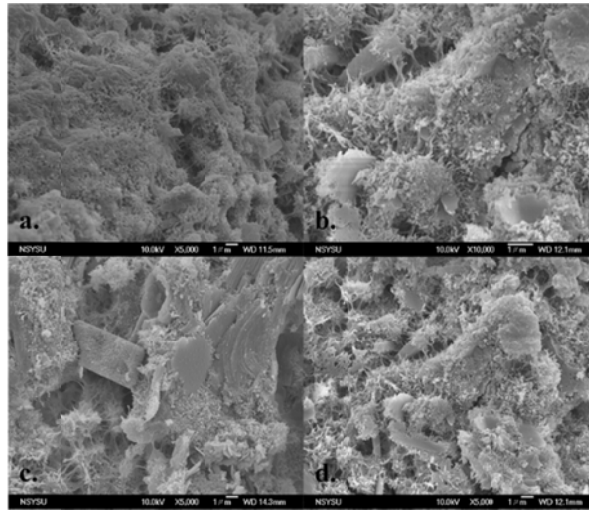


Fig. 12 The SEM microstructure of the DS low-strength steel slag mortar after high-temperature catalysis

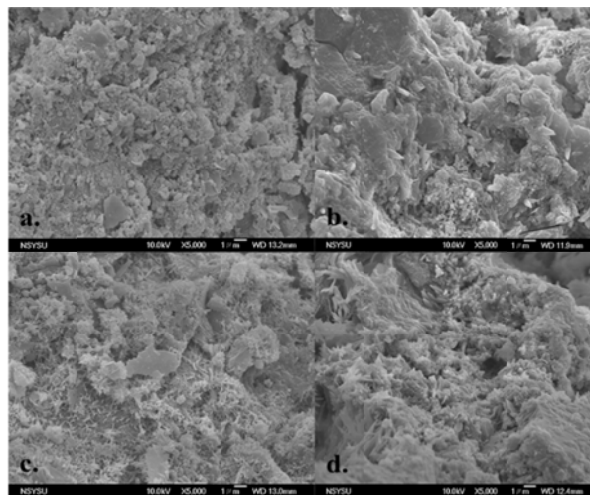


Fig. 13 The SEM microstructure of the low-strength BOF steel slag mortar after high-temperature catalysis

3.4 Scanning electron microscopy (SEM)

Fig. 12 shows the SEM microstructure of the DS low-strength steel slag mortar after high-temperature catalysis. Fig. 12(a) shows the result for the 20% DS sample. After 24 h of catalysis, a C-S-H colloid and laminar calcium hydroxide (CH) were observed, along with a small amount of lime (CaO), and the structure became more porous. Fig. 12(b) shows that after 72 h of catalysis, the amount of the C-S-H colloid increased as the amount of laminar calcium hydroxide (CH) decreased. Fig. 12(c) shows the image of the 30% DS sample after 24 h of high-temperature catalysis. In this case, laminar calcium hydroxide (CH) occupied most blocks, and the C-S-H colloid only occupied a small area. Fig. 12(d) shows that after 72 h of catalysis, the amount of the C-S-H colloid increased while the amount of laminar calcium hydroxide (CH) decreased. The 30% DS sample had more calcium hydroxide (CH) than the 20% DS sample. Fig. 13 shows the SEM microstructure of the low-strength BOF steel slag mortar after high-temperature catalysis. Fig. 13(a) shows the image of the 20% BOF specimen after 24 h of catalysis. A large amount of calcium hydroxide (CH) was observed, but no C-S-H colloid was apparent in the image. Fig. 13(b) shows that after 72 h of catalysis, the calcium hydroxide (CH) content increased, and the structure was compact. Fig. 13(c) shows the image of the 30% BOF specimen after 24 h of catalysis. The laminar calcium hydroxide (CH) and C-S-H colloid were found to intercross each other. Fig. 13(d) shows that after 72 h of catalysis, the calcium hydroxide (CH) content increased, but no C-S-H colloid was observed. Based on these results, similar hydrates of mostly laminar calcium hydroxide (CH) and a small amount of C-S-H colloid were produced after 24 h of catalysis regardless of the BOF content. After 72 h of catalysis, the hydration products varied as the BOF content increased. As the BOF content increased from 10% to 30%, the calcium hydroxide (CH) content decreased, and the amount of the C-S-H colloid increased in most cases. However, for BOF contents of 40% and 50%, the calcium hydroxide(CH) content increased, and the amount of the C-S-H colloid decreased to zero. In the DS sample with a higher f-CaO content, the micropores between the crystals were not filled with the C-S-H colloid or ettringite. The f-CaO hydration produced flaky calcium hydroxide crystals distributed throughout the bulk. As f-CaO was slowly hydrated, the calcium hydroxide crystals grew continuously, extruding peripheral hydration products (Mu *et al.* 2001). Therefore, the differential expansion pressure resulted in microcracks and initiated differential expansion burst. Under rapid catalysis at high temperatures, the calcium hydroxide crystals extruded peripheral hydration products instantly, making it difficult for the other hydration products to diffuse into the gaps between the flaky calcium hydroxide particles. The gaps between the crystals could not be filled, resulting in a local stress concentration and, eventually, deformation and cracking.

3.5 Comprehensive analysis

Figs. 5 and 8 show the volume expansion capacity results for the mortars with different amounts of steel slag after high-temperature catalysis. According to the trend curve, the expansion behavior of the DS mortar with a higher f-CaO content was more apparent than that of the BOF mortar with a lower f-CaO content after the high-temperature catalysis, indicating that the hidden f-CaO obviously expanded after the hydration was accelerated by the high temperature. This result is consistent with Kuo (Kuo and Shu 2014), the application of high-temperature catalytic technology can accelerate free lime reaction. When more than 20% of the natural river sand was replaced by DS, giving a mortar with a high f-CaO content, the samples fractured after 48 h of

catalysis. For the BOF mortars with lower f-CaO contents, fracturing did not occur until 30% of the natural river sand was replaced with BOF. The expansion capacity of the 20% BOF mortar was almost less than 0.9%. The DS mortar exhibited obvious swelling as the amount of DS increased. Based on the autoclave expansion results, when the expansion capacity exceeded 0.10%, fracturing occurred, the volume stability and durability were affected. The same trend was observed for the damage area ratios shown in Figs. 6 and 9. The damage area ratios of the stable mortars with less than 10% steel slag were less than 0.6%. However, when the damage area ratio was significantly higher than 0.8%, fracturing might have occurred.

4. Conclusions

This study suggested the standard recommended values and expansion fracture threshold values for the content of steel slag in controlled low-strength materials (CLSM), the results obtained are as follows

- The effects of the steel slag content varied based on the free lime content, but the percent of the natural river sand replaced by steel slag should not exceed 30%; otherwise, fracture failure might occur.
- Both the autoclave expansion and high-temperature catalysis results showed that fracturing occurred when the expansion capacity, which might influence the volume stability and durability, exceeded 0.10%. However, the expansion capacity was lower than 0.05% after tropical curing for 96 h, and no obvious deformation or damage was observed.
- The autoclave expansion showed that the expansion value of DS, which had a higher free lime content, was higher than that of the BOF. The steel slag was incompletely stabilized or overused, which affected the engineering durability severely.
- The damage area ratios of the stable mortars with less than 10% of the natural river sand replaced with steel slag were less than 0.6%. Fracturing might have occurred when the damage area ratio was greater than 0.8%.
- Although the high-temperature catalysis could briefly simulate the autoclave expansion acceleration, it took 96 h to obtain similar results. The equipment, however, is more universal than the autoclave expansion and operates safely. It can also be used at the same conditions as those employed in practical applications.
- Based on the SEM analysis, the calcium hydroxide crystals extruded peripheral hydration products instantly during the rapid high-temperature catalysis, resulting in a local stress concentration and, eventually, deformation and cracking.

Acknowledgements

The authors would like to thank the National Science Council of Taiwan for their financial support of this research under contract No. NSC 101-2221-E-151-065.

References

- Beaver Valley Slag, "www.bvslag.com/SlagExpansion.pdf".
- Cengiz, D.A., Alaettin, K. and Umur, K.S. (2004), "Strength and shrinkage properties of mortar containing a nonstandard high-calcium fly ash", *Cement. Concrete. Res.*, **34**(1), 99-102.
- Chatterji, S. (1995), "Mechanism of expansion of concrete due to the presence of dead- burnt CaO and MgO", *Cement. Concrete. Res.*, **25**(1), 51-56.
- Chaurand, P., Rose, J., Briois, V., Olivi, L., Hazemann, J.L., Proux, O., Domasf, J. and Bottero, J.Y. (2007), "Environmental impacts of steel slag reused in road construction: A crystallographic and molecular (XANES) approach", *J. Hazard. Mater.*, **139**(3), 537-542.
- Chen, F. (2011), "Application of detection for stability of concrete in concrete quality evaluation", *Fujian. Constr. Sci. Technol.*, **3**, 47-48.
- Hwang, C.L. (2010), *High Performance Concrete Theory and Practice*, Chans book, Taipei, Taiwan (in Chinese).
- Ivanka, N. (2011), "Utilisation of steel slag as an aggregate in concrete", *Mater. Struct.*, **44**(9), 1565-1575.
- Krittaya, K., Pitisan K., Taweechai S., Pongsak C. and Somnuk T. (2013), "Effect of free lime content on properties of cement-fly ash mixtures", *Constr. Build. Mater.*, **38**, 829-836.
- Kuo, W.T. and Shu, C.Y. (2014), "Application of high-temperature rapid catalytic technology to forecast the volumetric stability behavior of containing steel slag mixtures", *Constr. Build. Mater.*, **50**, 463-470.
- Li, C.M. and Li, W.J. (2005), "Discussion on quality and expansiveness of expansive material-magnesium oxide", *Des. Hydroelectric. Power. Station.*, **21**(3), 95-99.
- Lizarazo-Marriaga, J., Claisse, P. and Ganjian, E. (2011), "Effect of steel slag and portland cement in the rate of hydration and strength of blast furnace slag pastes", *J. Mater. Civil. Eng.*, **23**(2), 153-160.
- Lun, Y., Zhou, M., Cai, X. and Xu, F. (2008), "Methods for improving volume stability of steel slag as fine aggregate", *J. Wuhan. Univ. Technol. - Mater. Sci. Ed.*, **23**(5), 737-742.
- Mahmoud, A. (2012), "Laboratory studies to investigate the properties of CIR mixes containing steel slag as a substitute for virgin aggregates", *Constr. Build. Mater.*, **26**(1), 475-480.
- Montenegro, J.M., Celemin-Matachana, M., Cañizal, J. and Setién, J. (2013), "Ladle furnace slag in the construction of embankments: expansive behavior", *J. Mater. Civil. Eng.*, **25**(8), 972-979.
- Motz, H. and Geiseler, J. (2001), "Products of steel slags an opportunity to save natural resources", *Waste. Manage.*, **21**(3), 285-293.
- Mu, S.B., Sun, Z.Y. and Su, X.P. (2001), "A study on the microstructure and expanding mechanism of highly free-calcium oxide cements", *J. Wuhan. Univ. Technol.*, **23**(11), 27-30.
- Naganathan, S., Razak, H.A. and Nadzrian, A.H. (2010), "Effect of kaolin addition on the performance of controlled low-strength material using industrial waste incineration bottom ash", *Waste. Manage. Res.*, **28**(9), 848-860.
- Netinger, I. (2011), "Utilisation of steel slag as an aggregate in concrete", *Mater. Struct.*, **44**(9), 1565-1575.
- Qasrawi, H. (2009), "Use of low CaO unprocessed steel slag in concrete as fine aggregate", *Constr. Build. Mater.*, **23**(2), 1118-1125.
- Rafat, S. (2009), "Utilization of waste materials and by-products in producing controlled low-strength materials", *Resour. Conserv. Recy.*, **54**(1), 1-8.
- Rodriguez, A., Gutierrez-Gonzalez, S., Horgnies, M. and Calderon, V. (2013), "Design and properties of plaster mortars manufactured with ladle furnace slag", *Mater. Design.*, **52**, 987-994.
- Shen, D.H., Wu, C.M. and Du, J.C. (2009), "Laboratory investigation of basic oxygen furnace slag for substitution of aggregate in porous asphalt mixture", *Constr. Build. Mater.*, **23**(1), 453-461.
- Shi, C. and Qian, J. (2000), "High performance cementing materials from industrial slags-a review", *Resour. Conserv. Recy.*, **29**(3), 195-207.
- Sivakumar, N., Hashim, A.R., Siti, N. and Abdul, H. (2012), "Properties of controlled low-strength material made using industrial waste incineration bottom ash and quarry dust", *Mater. Design.*, **33**, 56-63.
- Svanera, M. (2012), "An innovative system for the re-use of slag from the electric arc furnace", *Metall.*

- Italiana.*, **2**, 37-43.
- Tareq, S. and Attar, A. (2013), "A mathematical model for predicting autoclave expansion for portland cement", *Impact. Factor.*, **4**(1), 110-116.
- Vagelis, G.P. (2000), "Effect of fly ash on portland cement systems: Part II. high-calcium fly ash", *Cement. Concrete. Res.*, **30**(10), 1647-1654.
- Wang, G. (2010), "Determination of the expansion force of coarse steel slag aggregate", *Constr. Build. Mater.*, **24**(10), 1961-1966.
- Wang, G. and Emery, J. (2004), "Technology of slag utilization in highway construction", *Proceedings of the Transportation Association on Annual Conference*, Québec, Canada.
- Wang, G., Wang, Y. and Gao, Z. (2010), "Use of steel slag as a granular material: volume expansion prediction and usability criteria", *J. Hazard. Mater.*, **184**(1-3), 555-560.
- Wang, X.Y. and Lee, H.S. (2014), "Prediction of compressive strength of Slag concrete using a blended cement hydration model", *Comput. Concrete.*, **14**(3), 247-262.
- Wang, Y.K. (2008), "Effect of basic oxygen furnace slag on porous asphalt concrete", M.S. thesis, National Cheng Kung Univ., Taiwan (in Chinese).
- World steel Association, *World steel in Figs.* 2013. Belgium. ISBN: 978-2- 930069-73-9.
- Wu, S., Xue, Y., Ye, Q. and Chen, Y. (2007), "Utilization of steel slag as aggregates for stone mastic asphalt (SMA) mixtures", *Build. Environ.*, **42**(7), 2580-2585.